Inorg. Chem. **2008**, *47*, 10499−10508

Magnetic Circular Dichroism Study of a Dicobalt(II) Methionine Aminopeptidase/Fumagillin Complex and Dicobalt II−II and II−III Model Complexes†

James A. Larrabee,* Seung-An Chyun, and Adam S. Volwiler

Department of Chemistry and Biochemistry, Middlebury College, Middlebury, Vermont 05753

Received June 23, 2008

The dicobalt form of the metallohydrolase methionine aminopeptidase from *Escherichia coli* (CoCo*Ec*MetAP) has an active site with one 5-coordinate Co^{II} and a more weakly bound 6-coordinate Co^{II}. These metal ions are bridged by two carboxylate amino acid side chains and water or hydroxide, potentially enabling magnetic exchange coupling between the metals. We used variable-temperature, variable-field magnetic circular dichroism to determine whether such coupling occurs. CoCo*Ec*MetAP's MCD spectrum shows distinct d−d transitions at 495 and 567 nm caused by 6- and 5-coordinate Co^{II}, respectively. The magnetization curves for 5- and 6-coordinate Co^{II} are very different, indicating that their electronic ground states vary considerably, ruling out any coupling. When the fungal metabolite fumagillin binds to the CoCoEcMetAP, the qualitative MCD spectrum is unchanged; however, VTVH MCD data show that 5- and 6-coordinate Co^{II} ions have similarly shaped magnetization curves, indicating that the Co^{II} ions now share the same electronic ground state. Fitting the VTVH MCD data to a model in which dimer wave functions are calculated using a spin Hamiltonian with zero-field splitting showed the Co^{II} ions to be weakly ferromagnetically coupled, with $J = 2.9$ cm^{-1}. Ferromagnetic coupling is unusual for dinuclear Co^{II}; therefore, to support the CoCoEcMetAP/fumagillin complex results, we also analyzed VTVH MCD data from a matched pair of dinuclear cobalt complexes, **1** and **2**. Complex **1** shares the carboxylate and hydroxide-bridged dicobalt(II) structural motif with the active site of CoCo*Ec*MetAP. Complex **2** contains a nearly isostructural Co^{II} ion, but the Co^{III} is diamagnetic, so any magnetic coupling is switched off, while the spectral features of the Co^{II} ion remain. Magnetization data for **1**, fitted to the dimer model, showed that the Co^{II} ions were weakly ferromagnetically coupled, with $J = 1.7$ cm^{-1}. Magnetization data for Co^{II} ions in **2**, however, reflect loss of magnetic exchange coupling.

Introduction

Methionine aminopeptidase (MetAP)[1] is a ubiquitous metallohydrolase responsible for removing the *N*-terminal methionine in nascent proteins.[1] Extensive studies on the dicobalt(II) form of the enzyme, CoCoMetAP, and structural determinations of human (CoCo*Hs*MetAP),[2] *Pyrococcus furious* (CoCo*Ps*MetAP),[3] and *Escherichia coli* (CoCo*Ec*MetAP)[4,5] MetAPs have revealed structurally similar dicobalt centers in the active sites. They consist of two metal ions bridged by water (or hydroxide), the carboxylate side groups from one aspartate, and one glutamate, both as μ-1,3 bridges. The active site structure in CoCo*Ec*MetAP has one Co^{II} ion (Co_1) pentacoordinated in a distorted trigonal-bipyramidal arrangement with imidazole nitrogen from histidine and a

* To whom correspondence should be addressed. E-mail: larrabee@middlebury.edu.

† Abbreviations used: MetAP, methionine aminopeptidase; *Ec*MetAP, *Escherichia coli* methionine aminopeptidase; CoCo*Ec*MetAP, dicobalt(II) *Escherichia coli* methionine aminopeptidase; CoCo*Ec*MetAP/F, fumagillin complex with dicobalt(II) *Escherichia coli* methionine aminopeptidase; VTVH MCD, variable-temperature variable-field magnetic circular dichroism; GpdQ, glycerophosphodiesterase from *Enterobacter aerogenes*; HEPES, 4-(2-hydroxyethyl)-1-piperazineethanesulfonic acid; CoCoAAP, aminopeptidase from *Aeromonas proteolytica*; AOM, angular overlap model; ZFS, zero-field splitting.

(1) Lowther, W. T.; Matthews, B. W. *Chem. Rev.* **2002**, *102*, 4581–4607.
(2) Liu, S.; Widom, J.; Kemp, C. W.; Crews, C. M.; Clardy, J. *Science* **1998**, *282*, 1324–1327.
(3) Tahirov, T. H.; Oki, H.; Tsukihara, T.; Ogasahara, K.; Yutani, K.; Ogata, K.; Izu, Y.; Tsunasawa, S.; Kato, I. *J. Mol. Biol.* **1998**, *284*, 101–124.
(4) Roderick, S. L.; Matthews, B. W. *Biochemistry* **1994**, *32*, 3907–3912.
(5) Lowther, W. T.; Orville, A. M.; Madden, D. T.; Lim, S.; Rich, D. H.; Matthews, B. W. *Biochemistry* **1999**, *38*, 7678–7688.

10.1021/ic8011553 CCC: $40.75
Published on Web 10/16/2008

Scheme 1

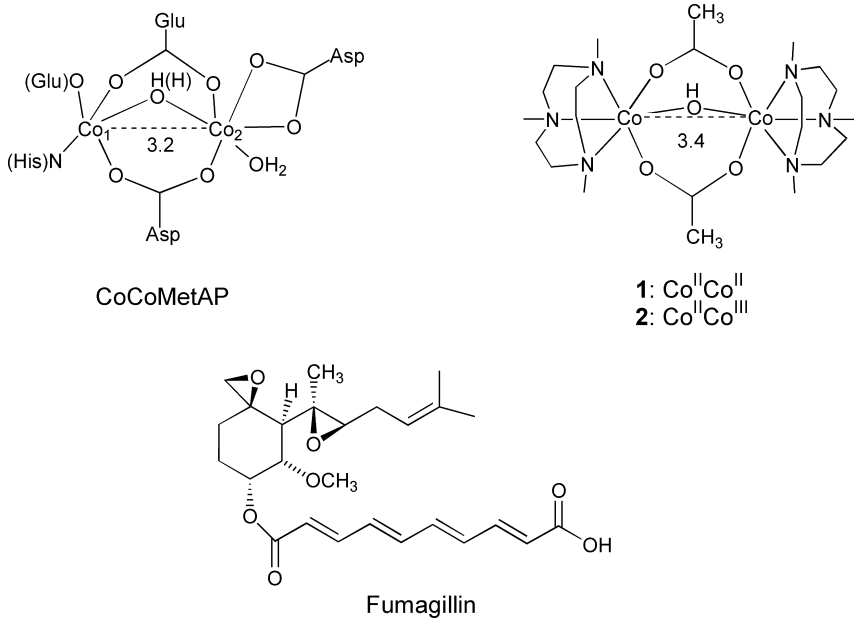

monodentate glutamate completing the coordination. The second Co^{II} ion (Co_2) is hexacoordinated in a distorted octahedral environment and has a coordinated water and bidentate aspartate completing its coordination sphere (Scheme 1). The binding affinities are different, and the Co_1 site has the greater binding affinity.[6] The μ-aqua/hydroxo, μ-carboxylato, dimetallic active site is a common structural motif in proteins and enzymes. Proteins other than MetAP that are in this category include the dioxygen carrier protein, hemerythrin, several phosphatases, aminopeptidase, phosphoesterases, and methane monooxygenases.[7−11] Because the activity of *Ec*MetAP peaks at a metal concentration at which only the metal binding site with greater affinity is fully occupied, it has been proposed that MetAP is a monometallic hydrolase.[6] Other evidence, principally crystallographic, points to MetAP being a dimetallic hydrolase.[1] A very recent study of inhibitor complexes with CoCo*Ec*MetAP hypothesized that the competing mono- and dimetallic mechanisms could be resolved by a third mechanism in which the second metal site becomes occupied only when substrate is present and then this metal leaves with product.[12] A substrate-induced, catalytically competent dimetallic active site mechanism has also been proposed in the structurally similar glycerophosphodiesterase from *Enterobacter aerogenes*, GpdQ.[13,14] In both the dimetallic and substrate-induced dimetallic mechanisms, the attacking nucleophile is the bridging water/hydroxide ligand that would be hyperactivated by serving as a ligand to two metal ions. Thus, it is of interest to know whether the actual bridging ligand is water or hydroxide. Furthermore, whether these enzymes have cobalt as the in vivo metal is doubtful, but most are fully active or even hyperactive in the cobalt form. *Ec*MetAP is likely a Mn^{II} or Fe^{II} enzyme,[15,16] and the in vivo metal for *Hs*MetAP is likely Mn^{II}.[17] Yet many of the chemical and structural studies have been conducted on the dicobalt forms of MetAP, and Co^{II} serves as an excellent spectroscopic probe of active site chemistry.

Because the μ-aqua/hydroxo, μ-carboxylato, dimetallic bridging core structure is a common enzyme active site structural feature, several dicobalt(II) model complexes have been reported with a bridging water[18−21] and bridging hydroxide.[22,23] One of the questions about CoCo*Ec*MetAP

(6) D'souza, V. M.; Bennett, B.; Copik, A. J.; Holz, R. C. *Biochemistry* **2000**, *39*, 3817–3826.
(7) Holmes, M. A.; Trong, I. L.; Turley, S.; Sieker, L. C.; Stenkamp, R. E. *J. Mol. Biol.* **1991**, *218*, 583–593.
(8) Wilcox, D. E. *Chem. Rev.* **1996**, *96*, 2435–2458.
(9) Holz, R. C. *Coord. Chem. Rev.* **2002**, *232*, 5–26.
(10) Mitić, N.; Smith, S. J.; Neves, A.; Guddat, L. W.; Gahan, L. R.; Schenk, G. *Chem. Rev.* **2006**, *106*, 3338–3363.
(11) Sazinsky, M. H.; Merkx, M.; Cadieux, E.; Tang, S.; Lippard, S. J. *Biochemistry* **2004**, *43*, 16263–16276.
(12) Evdokimov, A. G.; Pokross, M.; Walter, R. L.; Mekel, M.; Barnett, B. L.; Amburgey, J.; Seibel, W. L.; Soper, S. J.; Djung, J. F.; Fairweather, N.; Diven, C.; Rastogi, V.; Grinius, L.; Klanke, C.; Siehnel, R.; Twinem, T.; Andrews, R.; Curnow, A. *Proteins* **2007**, *66*, 538–546.
(13) Jackson, C. J.; Carr, P. D.; Liu, J.-W.; Watt, S. J.; Beck, J. L.; Ollis, D. L. *J. Mol. Biol.* **2007**, *367*, 1047–1062.
(14) Hadler, K. S.; Tanifum, E.; Yip, S. H.-C. ; Mitić, N.; Guddat, L. W.; Jackson, C. J.; Gahan, L. R.; Carr, P.; Ollis, D. L.; Hengge, A. C.; Larrabee, J. A.; Schenk, G. *J. Am. Chem. Soc.* submitted for publication.
(15) Meng, L.; Ruebush, S.; D'souza, V. M.; Copik, A. J.; Tsunasawa, S.; Holz, R. C. *Biochemistry* **2002**, *41*, 7199–7208.
(16) D'souza, V. M.; Brown, R. S.; Bennett, B.; Holz, R. C. *J. Biol. Inorg. Chem.* **2005**, *10*, 41–51.
(17) Wang, J.; Sheppard, G. S.; Lou, P.; Kawai, M.; Park, C.; Egan, D. A.; Schneider, A.; Bouska, J.; Lesniewski, R.; Henkin, J. *Biochemistry* **2003**, *42*, 5035–5042.
(18) Coucouvanis, D.; Reynolds, R. A.; Dunham, W. R. *J. Am. Chem. Soc.* **1995**, *117*, 7570–7571.
(19) Schultz, B. E.; Ye, B.-H.; Li, X.; Chan, S. I. *Inorg. Chem.* **1997**, *36*, 2617–2622.
(20) Brown, D. A.; Errington, W.; Glass, W. K.; Haase, W.; Kemp, T. J.; Nimir, H.; Ostrovsky, S. M.; Werner, R. *Inorg. Chem.* **2001**, *40*, 5962–5971.
(21) Turpeinen, U.; Ahlgren, M.; Hamalainen, R. *Acta Crystallogr.* **1982**, *B38*, 1580–1583.
(22) Chaudhuri, P.; Querbach, J.; Wieghardt, K.; Nuber, B.; Weiss, J. *J. Chem. Soc., Dalton Trans.* **1990**, 271–278.

Scheme 2. Hypothetical Structure of CoCo*Ec*MetAP/F Based on the Crystal Structure of CoCo*Hs*MetAP/F (PDB:1BOA)

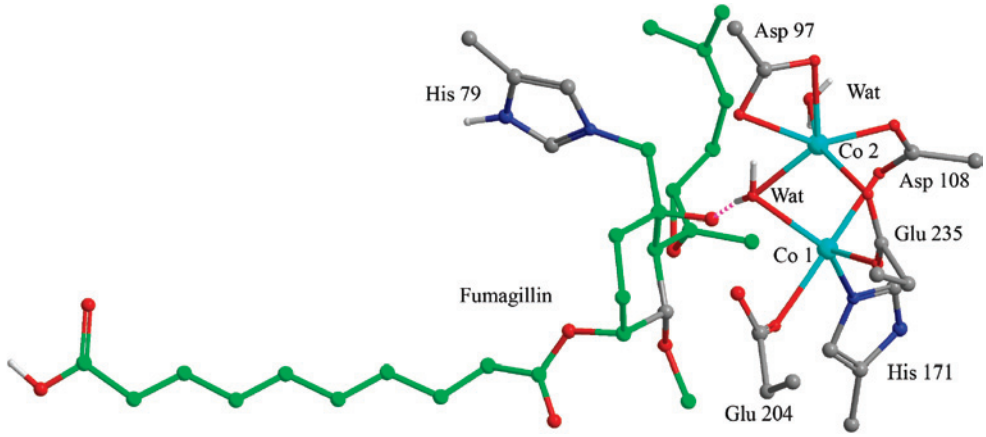

that might be answered by studying these model complexes is how to distinguish μ-aqua from μ-hydroxo. In these complexes, the Co^{II} ions are d^7 and high spin and weak magnetic exchange coupling through the bridging aqua/hydroxo ligand is expected. The strength of magnetic exchange coupling is usually defined using a spin Hamiltonian with an exchange coupling term of $-2JS_1 \cdot S_2$, where J gives the strength of magnetic exchange coupling and the sign of J indicates whether the magnetic coupling is ferromagnetic (positive) or antiferromagnetic (negative). On the basis of a study of magnetic exchange coupling in a series of μ-aqua and μ-hydroxo M^{II} complexes, where M = Mn, Ni, or Co, it was suggested that the magnitude of J will be less for μ-aqua complexes than it is for μ-hydroxo complexes.[19] Unfortunately, only μ-aqua data were reported for four Co^{II} complexes with J between -1.6 and -0.8 cm^{-1} for these complexes. In two other reports on μ-aqua, bis(μ-1,3-O_2CCH_3), dicobalt(II) complexes, J was found to be -0.2 and -0.7 cm^{-1}.[18,20] We could find no reports of J for dicobalt(II) complexes with a μ-hydroxo, bis(μ-carboxylato) bridging core structure; thus, a need exists to obtain data on these types of complexes to potentially develop useful correlations that might be applied to the study of CoCo*Ec*MetAP and other metallohydrolases.

To this end, we report on the investigation of magnetic exchange coupling in CoCo*Ec*MetAP, an inhibitor complex with the fungal metabolite, fumagillin (Scheme 1), CoCo*Ec*MetAP/F, and a model complex with a μ-hydroxo, bis(μ-carboxylato), dicobalt(II) bridging core structure, $[Co^{II}Co^{II}(\mu\text{-}O_2CCH_3)_2(\mu\text{-}OH)L_2]PF_6$ (**1**) (L = *N*′, *N*″, *N*‴-triazacyclononane, Scheme 1).[22] Varible-temperature, variable-field magnetic circular dichroism (VTVH MCD) is used to probe magnetic exchange coupling. A second complex, identical to **1** except that one of the cobalt ions is oxidized to Co^{III}, $[Co^{II}Co^{III}(\mu\text{-}O_2CCH_3)_2(\mu\text{-}OH)L_2](PF_6)_2$ (**2**, Scheme 1), is also included in this study. The pair of **1** and **2** is ideal for probing magnetic coupling because magnetic coupling can occur only in the $Co^{II}Co^{II}$ complex. The $Co^{II}Co^{III}$ complex contains an isostructural Co^{II} ion, but because Co^{III} is diamagnetic, the magnetic coupling is switched off while the spectral features of the Co^{II} remain. The VTVH MCD technique was recently applied to determine J in a similar matched pair of dicobalt complexes in which the metals are bridged by a pair of diphenylphosphates and a phenylate oxygen.[24] The Co^{II} ions in these complexes were weakly antiferromagnetically coupled with $J = -1.6$ cm^{-1}. Earlier EPR and MCD studies of CoCo*Ec*MetAP did not detect any magnetic coupling.[6,25] However, several structural studies of CoCoMetAP complexes with inhibitors and substrate analogs show bonding interactions with disruptions of the bridging water/hydroxide.[2,5,26,27] In such situations, it might be expected that weak magnetic exchange coupling, either ferromagnetic or antiferromagnetic, could be induced in CoCo*Ec*MetAP. Thus far, such coupling has not been demonstrated. Fumagillin complexes to MetAP by forming a covalent C−N bond to a histidine imdazole ring nitrogen near the active site through rupture of the ring epoxide.[2,18] A crystal structure of the CoCo*Hs*MetAP/fumagillin complex shows that the released alcoxide oxygen forms a hydrogen bond with the bridging water/hydroxide in the active site (Scheme 2).[2] The authors of this paper also suggested that this oxygen formed a bond to the cobalt in the Co_1 site, although at 3.28 Å the bond would be very weak.[2] An EPR study of a dimanganese(II) form of *Ec*MetAP found that the Mn^{II} ions were antiferromagnetically coupled.[16] Formation of the fumagillin complex had no effect on the exchange coupling, and fumagillin did not provide any ligands to the Mn^{II} ions. An EXAFS study on a fumagillin complex with CoCo*Ec*MetAP concluded that fumagillin does not provide a Co^{II} ligand and that possibly one of the two Co^{II} ions is displaced when fumagillin is bound.[28]

Experimental Section

Enzyme Preparation. *Ec*MetAP was prepared by a published procedure.[25,26] *Ec*MetAP was metallated to CoCo*Ec*MetAP by

(23) Mizoguchi, T. J.; Kuzelka, J.; Springler, B.; DuBois, J. L.; Davydov, R. M.; Hedman, B.; Hodgson, K. O.; Lippard, S. J. *Inorg. Chem.* **2001**, *40*, 4662–4673.
(24) Johansson, F. B.; Bond, A. D.; Nielsen, U. G.; Moubaraki, B.; Murray, K. S.; Berry, K. J.; Larrabee, J. A.; McKenzie, C. J. *Inorg. Chem.* **2008**, *47*, 5079–5092.
(25) Larrabee, J. A.; Leung, C. H.; Moore, R. L.; Thamrong-nawasawat, T.; Wessler, B. S. H. *J. Am. Chem. Soc.* **2004**, *126*, 12316–12324.
(26) Lowther, W. T.; McMillen, D. A.; Orville, A. M.; Matthews, B. W. *Proc. Natl. Acad. Sci. U.S.A.* **1998**, *95*, 12153–12157.
(27) Lowther, W. T.; Zhang, Y.; Sampson, P. B.; Honek, J. F.; Matthews, B. W. *Biochemistry* **1999**, *38*, 14810–14819.
(28) Cosper, N. J.; D'souza, V. M.; Scott, R. A.; Holz, R. C. *Biochemistry* **2001**, *40*, 13302–13309.

anaerobic dialysis against 50 mM KCl, 50 mM HEPES, pH 7.5, containing 1 mM Co(II) in a glovebox at 4 °C, as previously described.[25] Fumagillin-B was obtained from GloryBee Foods, Inc. as a mixture with sucrose. A saturated solution of Fumagillin-B was filtered and added to a solution of *Ec*MetAP. After incubation for 30 min at 30 °C, the solution was dialyzed against 50 mM KCl, 15 mM methionine, 50 mM HEPES, pH 7.5 to remove sucrose and excess fumagillin. The *Ec*MetAP/F was then concentrated, loaded into an anaerobic glovebox, and dialyzed against 50 mM KCl, 1 mM Co(II), 50 mM HEPES, pH 7.5. Formation of the CoCo*Ec*MetAP/F complex was verified by the presence of the characteristic intense UV absorption spectrum of fumagillin in the dialyzed material (Figure S1 in the Supporting Information).[26]

Model Complex Preparation. Complexes **1** and **2** were synthesized by the published procedure but using a Vacuum Atmospheres glovebox and solvents degassed by the freeze−pump−thaw method as additional precautions to avoid unintended oxidation of the Co(II).[22]

Spectroscopy. UV/vis/NIR absorption spectra were recorded using a Cary model 6000i spectrometer. Absorption spectra of **1** and **2** were recorded as ethanolic solutions using ethanol that was degassed by the freeze−pump−thaw method. Samples were loaded in a glovebox into screw-cap cuvettes. All samples were freshly prepared before MCD data were collected. The MCD sample cell (previously described) was loaded inside a glovebox and then directly placed into the SM4 or SM4000 cryostat/magnet.[25] The MCD system used has a JASCO J600 spectropolarimeter and an Oxford Instruments SM4 cryostat/magnet, which was recently replaced by an Oxford Instruments SM4000 cryostat/magnet. Because three separate sample preparations were conducted for each sample, followed by VTVH MCD data collection, data were collected on both versions of MCD systems. The protocol for VTVH MCD data collection has been previously described.[25] Data were collected at increments of 0.5 T (T) from 0 to 7.0 T and at temperatures of 1.5, 3.0, 4.2, 6.0, 10, 20, and 50 K. MCD spectra of complexes **1** and **2** were collected as frozen ethanolic glasses. MCD spectra of the enzymes were collected as frozen glasses formed from 60/40 (v/v) glycerol/aqueous 50 mM KCl, 1 mM Co^{II}, 50 mM HEPES, pH 7.5. VTVH MCD intensity data were corrected for any residual CD at zero field and, in the case of CoCo*Ec*MetAP samples, any MCD intensity caused by unbound Co^{II}. The latter is a very small correction because the intensity of free aqueous Co^{II} is about 100-fold lower on a per molar basis than that of Co^{II} bound in the 6-coordinate site.

Angular Overlap Calculations. Angular overlap model (AOM) calculations were made using AOMX, a program based on routines developed by Hoggard for d^3 transition metal ions and extended to d^n systems by Adamsky.[29] AOMX determines the optimum ligand field parameters needed to fit an observed set of d−d transitions based on a given structure. Input to AOMX requires the ligand coordinates referred to the metal ion at the origin. The coordinates for the Co^{II} ligand set were taken directly from the published crystal structure. The Co^{II} ligand set was assumed to be three equivalent nitrogens, two equivalent oxygens from the bridging acetate groups, and the unique hydroxide bridging oxygen. AOMX does not use the bond distances to fit the spectrum; only the bond angles are important, and these are fixed by the crystal structure. However, the bond distances are reflected by the magnitude of the resulting ligand field parameters, ϵ_σ and ϵ_π.

MCD Data Analysis. VTVH MCD data were normalized to the maximum observed intensity and fitted using a Simplex algorithm that minimizes a chi-squared goodness of fit parameter. Two complimentary models, a dimer model and a singlets/doublets model, were used in fitting the data for magnetically coupled $Co^{II}Co^{II}$ non-Kramers systems. In the dimer model, wave functions are calculated using a spin Hamiltonian (Equation S1 in the Supporting Information), and the MCD intensity is given by the spin expectation values of the Co^{II} ion responsible for the MCD transition. The dimer model yields the coupling constant, J, the single-ion zero-field splitting parameters, D and E, the polarization of the transition, and the energies and total M_S values of the resulting wave functions. The g and D tensors are collinear, and the polarization of the transition is relative to these tensors. For two high-spin Co^{II} ions, the dimer model yields 16 sublevels. The second fitting procedure uses a singlet and doublet model for non-Kramers (integral spin) or Kramers (nonintegral spin) systems that includes an orientation-averaged MCD intensity expression, allowing for linear B terms from field-induced mixing between states and the presence of thermally populated sublevels above the ground state (Equation S2 in Supporting Information). The singlets/doublets model yields the effective g for each doublet, the zero-field splitting in the dimer (non-Kramers system), δ, the energy of each level, and the M_z/M_{xy} polarization ratio. The models, theory, equations, and computer programs to fit the VTVH MCD data have been developed by the Solomon group over the past several years and are described in detail elsewhere.[30−35] The computer programs and instruction for using them were kindly provided Dr. Nataša Mitić, a former member of the Solomon group who is currently located at University of Queensland, Australia.

Fitting VTVH MCD data from a coupled ($J \neq 0$) system using these two models/programs is an iterative process because the energy and total M_S of each sublevel given by the dimer model must be consistent with the energy and effective g given by the singlets/doublets model. Excellent descriptions of this process for coupled diiron(II) systems have been published.[34,35] In the coupled dicobalt(II) systems described in this study and in a previous study on a weakly antiferromagnetically coupled dicobalt(II) complex[24] we found that it was better to fit the data to the dimer model first and determine which energy levels would be populated at low temperatures and what the total M_S was for each of these levels. The energy and appropriate effective g were then set as a starting point when fitting the data to using the singlets/doublets program.

The VTVH MCD data from Kramers systems (nonintegral spin, uncoupled Co^{II}) were fitted using the same singlets/doublets program, but the value for δ is fixed at zero, and only doublets were defined. The VTVH MCD data sets that were fitted included all temperatures, nominally 1.5, 3.0, 4.2, 10, 20, and 50 K; however, typically only three isotherms (at 1.5, 4.2, and 10 K) are shown in the figures for clarity.

(29) (a) Hoggard, P. E. *Top. Curr. Chem.* **1994**, *171*, 113–141. (b) The AOMX program is maintained and distributed by H. Adamsky, Institut fur Theoretische Chemie, Heinrich Heine Universitat, Duesseldorf, Germany; e-mail adamsky@theochem.uni-duesseldorf de. The AOMX program and complete documentation are available at http://www.aomx.de, which was last accessed by the corresponding author on July 29, 2008.

(30) Reem, R. C.; Solomon, E. I. *J. Am. Chem. Soc.* **1987**, *109*, 1216–1226.

(31) Solomon, E. I.; Pavel, E. G.; Loeb, K. E.; Campochiaro, C. *Coord. Chem. Rev.* **1995**, *144*, 369–460.

(32) Neese, F.; Solomon, E. I. *Inorg. Chem.* **1999**, *38*, 1847–1865.

(33) Strand, K. R.; Yang, Y.-S.; Andersson, K. K.; Solomon, E. I. *Biochemistry* **2003**, *42*, 12223–12234.

(34) Wei, P.; Skulan, A. J.; Mitić, N.; Yang, Y.-S.; Saleh, L.; Bollinger, J. M.; Solomon, E. I. *J. Am. Chem. Soc.* **2004**, *126*, 3777–3788.

(35) Wei, P.; Tomter, A. B.; Rohr, A. K.; Andersson, K. K.; Solomon, E. I. *Biochemistry* **2006**, *45*, 14043–14051.

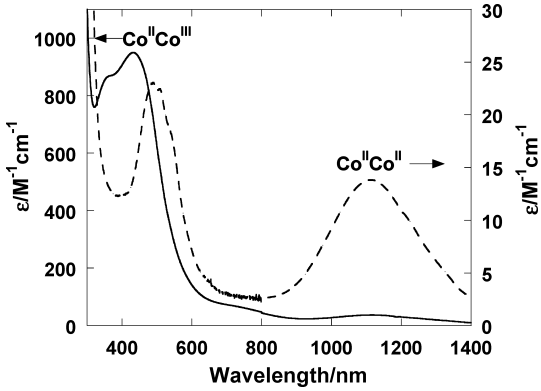

Figure 1. Absorption spectra of **1** (dashed line) and **2** (solid line) in ethanol.

Results

Results are presented first for **1** and **2** because this matched pair of model complexes provides an example of how VTVH MCD is used to detect a change in the electronic ground state on going from the $Co^{II}Co^{III}$ (**2**) to the $Co^{II}Co^{II}$ (**1**) dimer. The change that is observed in the magnetization plots of the VTVH MCD data must be attributed to magnetic exchange coupling, which is weakly ferromagnetic. The results of the model complex study are then used to support the VTVH MCD analysis of CoCo*Ec*MetAP and CoCo*Ec*-MetAP/F.

Excited States of Co^{II} in 1 and 2. Figure 1 shows the room-temperature absorption spectra of ethanol solutions of **1** and **2**. In the spectrum of the $Co^{II}Co^{II}$ complex **1** a cluster of three overlapping bands at 483, 510, and 548 nm and a broad near-infrared band at 1115 nm are typical for hexacoordinate Co^{II}.[36] The near-IR band arises from the $^4T_{1g} \rightarrow {}^4T_{2g}$ d−d transition in O_h symmetry, and the visible absorption arises from the $^4T_{1g} \rightarrow {}^4T_{1g}(P)$ d−d transition in O_h symmetry, which is split into three bands by geometric distortion from O_h. The local symmetry, considering only the cobalt and first coordination sphere atoms, is no higher than C_{2v}. Considerable ligand field heterogeneity is present as well (vide infra), which also contributes to the splitting of this transition. The spectrum of the $Co^{II}Co^{III}$ complex (**2**) is very different in that the visible band at 432 nm with a shoulder at 367 nm is 400-fold more intense than the visible bands in **1**. This intensity completely swamps any d−d arising from the Co^{II} and is likely the result of both charge-transfer and d−d transitions from the Co^{III} ion.[22] The near-IR transition from the Co^{II} ion is still readily apparent in **2**.

Figure 2 shows the visible region MCD spectra of **1** and **2** in frozen ethanol glasses. The solubility of **2** in ethanol is considerably greater than that of **1**; thus, even though the $\Delta\epsilon$ for the transitions arising from Co^{II} is doubled in **1** compared to **2**, better signal-to-noise was obtained on MCD spectra of **2** than for **1**. The observed peaks in both **1** and **2** are temperature-dependent C terms, including the very weak peaks around 400 nm, indicative of transitions originating from a paramagnetic ground state; thus, only the peaks

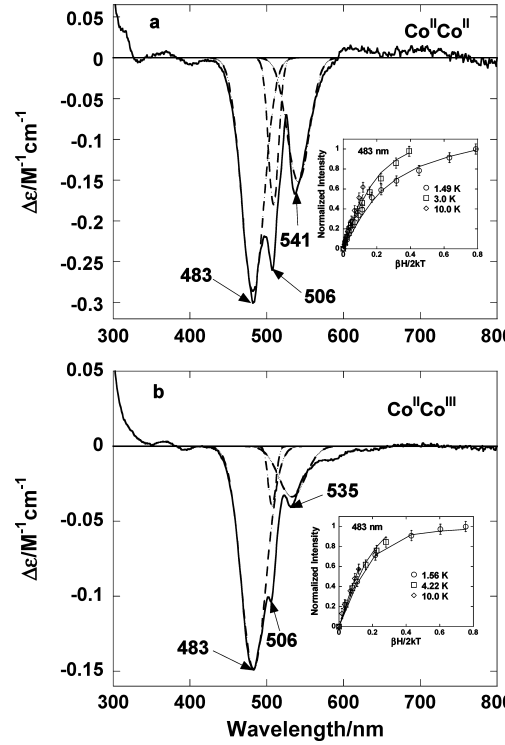

Figure 2. MCD spectra of **1** (a) and **2** (b) in frozen ethanol glass at 1.5 K and 3.5 T. Dashed lines represent three Gaussian components of the major band. The inset to a is the magnetization plot of the 483 nm peak from **1**. The solid lines represent the best fit using the dimer model with the parameters listed in Table 3. The inset to b is the magnetization plot of the 483 nm peak from **2**. The solid lines represent the best fit to an isolated doublet with the parameters listed in Table 2.

caused by d−d transitions of the paramagnetic Co^{II} are observed. Furthermore, the fact that the d−d transitions from Co^{II} in the MCD spectra of **1** and **2** can be virtually superimposed confirms that the charges on the Co^{II} are localized in **1** and **2**, and by implication, the charge is also localized on the Co^{III} in **2**.[21] The three bands are at 483, 506, and 541 nm in **1** and at 483, 506, and 535 nm in **2**. These patterns closely correspond to those observed in the absorption spectrum of **1**.

Ligand field calculations using the angular overlap model (AOM) help to confirm assignment of the Co^{II} d−d transitions in **1** and **2**.[29,37,38] In these calculations, the positions of the Co^{II} ligands are taken from the published crystal structure of **2**. The AOMX program adjusts the ligand field strength parameters ϵ_σ and ϵ_π to obtain the best fit to the experimental spectrum. The data are not sufficient to calculate ϵ_σ and ϵ_π for each ligand, even assuming that the two acetate oxygen atoms are equivalent and that the three amine nitrogen atoms are equivalent. Thus, we initially assumed that π bonding between the ligands and Co^{II} was zero. This is an excellent assumption for the amine and acetate ligands, but π-bonding interactions can be important for metal−hydroxide bonds.[38,39] Nevertheless, the AOMX

(36) Lever, A. B. P. *Inorganic Electronic Spectroscopy*, 2nd ed.; Elsevier: Amsterdam, 1984; pp 479−503.

(37) Figgis, B. N.; Hitchman, M. A. *Ligand Field Theory and Its Applications*; Wiley-VCH: New York, 2000; pp 53−82.

(38) Hoggard, P. E. *Struct. Bonding (Berlin)* **2004**, *106*, 37–57.

(39) Lever, A. B. P.; Walker, I. M.; McCarthy, P. J.; Mertes, K. B.; Jircitano, A.; Sheldon, R. *Inorg. Chem.* **1983**, *22*, 2252–2258.

Table 1. Vis/NIR Absorption, MCD, and AOM Calculations for **1** and **2**

	vis/NIR[a] λ_{max} [nm] (ϵ)[$M^{-1}cm^{-1}$]	MCD[b] λ_{max} [nm] ($\Delta\epsilon$) [$M^{-1}cm^{-1}$]	calcd[c]	origin of Co^{II} d−d in O_h
1		367(+0.006)		$^4T_{1g} \rightarrow$ doublet Co^{II}
		401(−0.008)		$^4T_{1g} \rightarrow$ doublet Co^{II}
	484(22.9)	483(−0.30)	483	$^4T_{1g} \rightarrow {}^4T_{1g}(P)$ Co^{II}
	510(22.1)	506(−0.26)	510	$^4T_{1g} \rightarrow {}^4T_{1g}(P)$ Co^{II}
	548(17.5)	541(−0.17)	537	$^4T_{1g} \rightarrow {}^4T_{1g}(P)$ Co^{II}
			591	$^4T_{1g} \rightarrow {}^4A_{2g}$ Co^{II}
	1115(13.9)		1180	$^4T_{1g} \rightarrow {}^4T_{2g}$ Co^{II}
2	367(873)			Co^{III} d−d + CT
	432(950)			Co^{III} d−d + CT
	700(74)			Co^{III} d−d
		367(+0.003)		$^4T_{1g} \rightarrow$ doublet Co^{II}
		394(−0.003)		$^4T_{1g} \rightarrow$ doublet Co^{II}
		483(−0.15)	483	$^4T_{1g} \rightarrow {}^4T_{1g}(P)$ Co^{II}
		506(−0.10)	510	$^4T_{1g} \rightarrow {}^4T_{1g}(P)$ Co^{II}
		535(−0.04)	537	$^4T_{1g} \rightarrow {}^4T_{1g}(P)$ Co^{II}
		588(−0.009)	591	$^4T_{1g} \rightarrow {}^4A_{2g}$ Co^{II}
	1115(22)		1180	$^4T_{1g} \rightarrow {}^4T_{2g}$ Co^{II}

[a] In EtOH at 25 °C. [b] In frozen EtOH glass; $\Delta\epsilon$ for sample at 1.5 K and 3.5 T. [c] AOMX parameters (cm^{-1}): $\epsilon_\sigma(OH^-) = 6000$, $\epsilon_\sigma(OAc^-) = 2680$, $\epsilon_\sigma(N) = 3225$, $B = 796$.

Table 2. Best Fit Parameters of the VTVH MCD Data from **2** to a Doublet Using the Singlets/Doublets Model

parameter	483 nm peak	506 nm peak	535 nm peak
$g_{\|\|}$	5.0	5.1	5.2
A_{satlim}	3.6	3.0	3.7
B	0.04	0.05	0.09
$g_\perp$	2.0	2.0	2.0
M_z/M_{xy}	0.29	0.24	0.37

Table 3. Best Fit Parameters of the VTVH MCD Data from **1** to the Dimer Model

parameter	483 nm peak	506 nm peak	541 nm peak
J	1.7 cm^{-1}	1.3 cm^{-1}	1.7 cm^{-1}
D_1, D_2	60 cm^{-1}	60 cm^{-1}	60 cm^{-1}
E_1, E_2	0	0	0
$M_x{}^a$	91%	2.8%	98%
$M_y{}^a$	7.5%	81%	1.7%
$M_z{}^a$	1.5%	16.2%	0.3%

[a] Calculated from M_{xy}, M_{yz}, and M_{xz} according to $\%x = (M_{xy}\cdot M_{xz})^2/(M_{xy}\cdot M_{xz})^2 + (M_{xy}\cdot M_{yz})^2 + (M_{xz}\cdot M_{yz})^2$. Calculation of the y and z polarizations is done correspondingly.[46]

fit was found to be excellent and is summarized in Table 1 along with the absorption and MCD spectral data. After the best fit was obtained assuming that all ϵ_πs were zero, the carboxylate and amine values for ϵ_σ were locked in and ϵ_σ and ϵ_π for hydroxide was allowed to float; however, this approach did not improve the fit.

What might first appear to be an anomaly is that ϵ_σ for the amine nitrogen is smaller (3225 cm^{-1}) than ϵ_σ for hydroxide (6000 cm^{-1}) and only slightly larger than ϵ_σ for acetate oxygen (2680 cm^{-1}). However, the Co^{II}−N bond distances are 2.18 Å, while the Co^{II}−O(acetate) bonds are shorter at 2.08 Å, and the Co^{II}−O(hydroxide) bond is shortest at 2.03 Å. Investigations have shown that ϵ_σ decreases as $\sim 1/r^6$ for amine ligands, which can account for the low value for ϵ_σ found for the amine ligands.[39] The results of the AOM analysis emphasize the ligand field heterogeneity around the Co^{II} ions in these complexes. This heterogeneity results in a large splitting of the $^4T_{1g}$ (in O_h) ground state into three orbital singlets/spin quartets at 0, 718, and 1490 cm^{-1}, which quenches orbital angular momentum. The AOM analysis also

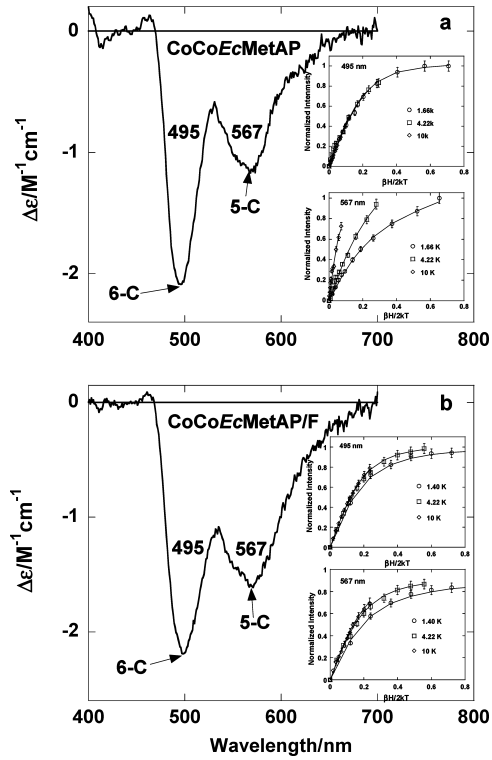

Figure 3. MCD Spectra of CoCo*Ec*MetAP (a) and CoCo*Ec*MetAP/F (b) in frozen 60/40 glycerol/buffer glasses at 1.5 K and 3.5 T. Insets to a are magnetization plots of the 495 and 567 nm peaks. Solid lines represent the best fit to the singlets/doublets model with parameters listed in Table 6. Insets to b are magnetization plots of the 495 and 567 nm peaks. Solid lines represent the best fit to the dimer model with parameters listed in Table 7.

determined that six doublet states are between 24 500 and 27 000 cm^{-1}; these findings can account for the weak, temperature-dependent peaks observed in the MCD of **1** at 367 and 401 nm and in **2** at 367 and 394 nm. It is not uncommon for the intensity of spin-forbidden d−d transitions to be enhanced in the MCD spectrum, as demonstrated by some Cr^{III} complexes.[40,41] The temperature dependence of these two bands rules out the possibility that they could be caused by Co^{III}, even though the Co^{III} has very strong absorptions at these wavelengths.

Excited States of CoCoEcMetAP and CoCoEcMetAP/F. Figure 3 shows the MCD spectra, taken at low temperature, of CoCo*Ec*MetAP and CoCo*Ec*MetAP/F, which are identical within the ±2 nm spectral bandwidth. The broad band at 567 nm and a shoulder at 625 nm are attributed to d−d transitions on the 5-coordinate Co^{II}, which occupies the high-affinity Co_1 site.[25] The other band, at 495 nm, is a d−d transition on the 6-coordinate Co^{II}, which occupies the Co_2 site.[25] Comparing the ratio of protein absorption at 280 nm to fumagillin absorption at 340 nm (Figure S1, Supporting Information) in the UV/visible absorption spectrum of CoCo*Ec*MetAP/F (Figure S1, Supporting Information) with the published spectrum indicates that the fumagillin in

(40) Schreiner, A. F.; Hauser, P. J. *Inorg. Chem.* **1972**, *11*, 2706–2713.
(41) Hauser, P. J.; Schreiner, A. F.; Evans, R. S. *Inorg. Chem.* **1974**, *13*, 1925–1927.
(42) Johnson, M. K. In *Physical Methods in Bioinorganic Chemistry*; Que, L. , Ed.; University Science: Sausalito, CA, 2000; Chapter 5.

Table 4. Energy Levels and Spins for the 16 Sublevels in the Ground State of **1**

energy [cm^{-1}]	S_{total}, $\lvert M_{s\ total}\rvert$
0	3, 0
3.7	3, 1
10.5	1, 0
118.8	3, 2
126.6	2, 0
126.6	2, 2
126.9	2, 1
238.8	3, 3
250.6	1, 1
250.6	0, 0

Table 5. Best Fit Parameters of the VTVH MCD Data from **1** to the Singlets/Doublets Model

parameter	483 nm peak	506 nm peak	541 nm peak
singlet 1 (g.s.)			
B	0.7	0.5	0.5
doublet			
energy	3.7 cm^{-1}	3.7 cm^{-1}	3.7 cm^{-1}
δ	<0.1 cm^{-1}	<0.1 cm^{-1}	<0.1 cm^{-1}
$g_{\|\|}$	4.3	4.3	4.3
A_{satlim}	−28.5	−14.4	−13.6
B	0.28	0.25	0.35
$g_{\perp}$	2	2	2
M_z/M_{xy}	0.6	0.6	0.6
singlet 2			
energy	10.5 cm^{-1}	10.5 cm^{-1}	10.5 cm^{-1}
B	−1.2	−1.0	−1.1

Table 6. Best Fit Parameters of the VTVH MCD Data from CoCo*Ec*MetAP to the Singlets/Doublets Model

parameter	495 nm peak	567 nm peak
doublet 1 (g.s.)		
$g_{\|\|}$	5.9	6.0
A_{satlim}	2.4	1.3
B	0.008	0.1
$g_{\perp}$	2.0	2.0
M_z/M_{xy}	0.04	0
doublet 2		
energy		18.7 cm^{-1}
$g_{\|\|}$		2.0
A_{satlim}		768
B		−9.5
$g_{\perp}$		2.0
M_z/M_{xy}		0

CoCo*Ec*MetAP/F is nearly stoichiometric.[26] The fact that the qualitative MCD spectrum did not change upon fumagillin binding suggests that fumagillin does not provide any ligands to either cobalt nor does it cause any major disruption to the bridging core. This finding is completely in line with a conclusion from an EPR study of the dimanganese *Ec*MetAP/fumagillin complex.[16]

Ground States of Co^{II} in 1 and 2. The inset to Figure 2b shows the magnetization of the MCD signal in the low-temperature regime for the 483 nm peak in **2**. (The magnetization plots for the 506 and 535 nm peaks are given in Figures S7 and S8 in the Supporting Information.) The magnetization isotherms nearly overlay, and the overall shape is independent of wavelength. This is typical behavior for MCD transitions from an isotropic Kramers doublet.[42] The Co^{II} in **2** is an isolated distorted 6-coordinate high-spin d^7species. Because the Co^{III} is diamagnetic, no magnetic coupling is possible. The orbital degeneracy of the $^4T_{1g}$ ground state (in octahedral symmetry) is lifted by geometric distortion and ligand heterogeneity, as confirmed by the AOM results. The distorted Co^{II} ion will have a spin quartet, orbital singlet ground state. The quartet is subject to zero-field splitting (ZFS), which is large for 6-coordinate Co^{II}, and the ground-state splits into two pseudo-Kramers doublets, separated by the total ZFS, which usually exceeds 100 cm^{-1} (total ZFS = $2D$ if E is zero).[43−45] In the low-temperature regime, only the lower doublet will be populated. Thus, the magnetization isotherms take the shape of an isolated pseudo-Kramers doublet. The VTVH MCD data were fitted to a single doublet using the singlets/doublets program with the parameters given in Table 2. The fit to the 483 nm data is shown in the inset to Figure 2b. The fits to the 506 and 535 nm data are shown in Figures S7 and S8 in the Supporting Information. Although the effective $g \approx 5$ is close to a predicted value of 6 for a ground state with $M_s = \pm 3/2$, this value cannot be relied upon to determine the sign of D. The mixing between the $M_s = \pm 3/2$ and $M_s = \pm 1/2$ levels makes the sign ambiguous.[45]

Table 7. Best Fit Parameters of the VTVH MCD Data from CoCo*Ec*MetAP/F to the Dimer Model

parameter	495 nm peak	567 nm peak
J	2.9 cm^{-1}	3.4 cm^{-1}
D_1	60 cm^{-1}	−9.4 cm^{-1}
D_2	−9.4 cm^{-1}	60 cm^{-1}
E_1, E_2	0, 0	0, 0
M_x[a]	85%	100%
M_y[a]	11%	0
M_z[a]	4%	0

[a] Calculated from M_{xy}, M_{yz}, and M_{xz} according to $\%x = (M_{xy}\cdot M_{xz})^2/(M_{xy}\cdot M_{xz})^2 + (M_{xy}\cdot M_{yz})^2 + (M_{xz}\cdot M_{yz})^2$. The y and z polarizations are calculated correspondingly.[46]

The inset to Figure 2a shows the magnetization plot for the 483 nm band in **1**. The magnetization plots for the 506 and 541 nm peaks are shown in Figures S2−S6 in the Supporting Information. The isotherms do not nearly overlay as for **2** but are more nested. This discrepancy is clear evidence that the ground states of the Co^{II} in **1** and **2** are different. The Co^{II} ions in **1** no longer have isolated doublet ground states, as the Co^{II} ion in **2** does, because magnetic exchange coupling is now occurring between them through the bridging hydroxide. The ground state is described by the spin Hamiltonian given in Equation S1, Supporting Information, which yields 16 sublevels. Because the ZFS is so large, only a few of these levels will be populated at low temperatures. The VTVH MCD data from **1** were fitted to the dimer model equation, and the best fit parameters are summarized in Table 3. The dimer model fit to the 483 nm band data is shown in the inset to Figure 2a, and the dimer model fits to the 506 and 541 nm band data are shown in Figures S3 and S4, Supporting Information, respectively. The fit was not very sensitive to D as long as $D > 40$ cm^{-1},

(43) Duggan, D. M.; Hendrickson, D. N. *Inorg. Chem.* **1975**, *14*, 1944–1956.
(44) Bossek, U.; Nuhlen, D.; Bill, E.; Glaser, T.; Krebs, C.; Weyhermuller, T.; Wieghardt, K.; Lengen, M.; Trautwein, A. X. *Inorg. Chem.* **1997**, *36*, 2834–2843.
(45) Larrabee, J. A.; Alessi, C. M.; Asiedu, E. T.; Cook, J. O.; Hoerning, K. R.; Klingler, L. J.; Okin, G. S.; Santee, S. S.; Volkert, T. L. *J. Am. Chem. Soc.* **1997**, *119*, 4182–4196.

which was the case. No reasonable fit was possible if the sign of D was negative, so the sign of D was always fixed as positive for 6-coordinate Co^{II}. Once the values for J and D were locked in, floating E did not improve the fits, so E was set to zero. The fits to the dimer model are excellent for all three peaks, and the agreement for J is good. The 506 nm peak is overlapped on both sides, so the value for that J is considerably less reliable. The energy and total M_s for each of the 16 sublevels that result from weak ferromagnetic coupling and strong ZFS ($J = 1.7$ cm^{-1} and $D = 60$ cm^{-1}) are given in Table 4. Only four sublevels, a singlet ground state, a doublet at 3.6 cm^{-1}, and another singlet at 10.5 cm^{-1}, will be populated at the low temperatures of the MCD experiment.

An alternate explanation for the difference in the nesting of the magnetization curves of **1** and **2** is that the polarization of the bands has changed, and this scenario was proposed by two of the reviewers of the draft manuscript. To test this hypothesis, the VTVH MCD data of the 483 nm peak of complex **1** were fitted using the dimer program, letting the polarization float and fixing $J = 0$. The results are shown in the Supporting Information, Figure S11. The chi-squared goodness of fit parameter nearly tripled, primarily because the lowest temperature data, taken at 1.49 K, did not fit well at all. This result maybe is not surprising in light of the fact that $M_s = 0$ for the lowest sublevel in **1** for the ground state with $J = 1.7$ cm^{-1} and $D = 60$ cm^{-1}, whereas for the ground state with $J = 0$, the lowest sublevel in **1** would have $M_s = \pm 3/2$ on each cobalt ion.

The coupled Co^{II} ions in **1** constitute a non-Kramers system subject to ZFS of the dimer doublet states, δ. The VTVH MCD data were fitted using the singlets/doublets program, allowing for only two singlet states at 0 and 10.5 cm^{-1} and one doublet state at 3.7 cm^{-1}. The results from the dimer fit indicate that the transitions should be x- or y polarized, and the effective g should be $\sim$4, which is the case. The best fit parameters of the VTVH MCD data for the three bands are given in Table 5. The fits are shown in Figures S2−S4 in the Supporting Information.

Ground States of Co^{II} in CoCoEcMetAP and CoCoEcMetAP/F. The insets to Figure 3a show the magnetization plots for the 495 and 567 nm MCD peaks from CoCo*Ec*MetAP. The isotherms in the magnetization data for the 495 nm peak can be virtually superimposed and are consistent with a nearly isotropic pseudo-Kramers doublet, which is expected for high-spin 6-coordinate Co^{II} (in the Co_2 site). This observation is also analogous to the magnetization behavior of the VTVH MCD data from the Co^{II} in **2**. Thus, these data were fitted to an isolated doublet using the singlets/doublets program. The best fit parameters are given in Table 6, and the fit is shown in the Figure 3a inset. The magnetization of the 567 nm band has a very different shape with the isotherms nested. The different shape immediately suggests that the two Co^{II} ions do not share the same ground state, which means they are not coupled. High-spin 5-coordinate Co^{II} will have a ^{4}A ground state regardless of formal symmetry. The Co_1 site is close to trigonal-bipyramidal geometry, but the ligand field is very heterogeneous.[17] ZFS will split the ground-state spin quartet into $M_s = \pm 3/2$ and $M_s = \pm 1/2$ doublets. The separation of the doublets will be $2|D|$ (assuming $E = 0$), and the sign of D will be positive if the $M_s = \pm 1/2$ doublet is lower (g effective $\approx$ 2) and negative if the $M_s = \pm 3/2$ is lower (g effective $\approx$ 6).[37] Thus, fitting the VTVH MCD data from the 567 nm peak yields the magnitude and sign of the ZFS for the 5-coordinate Co^{II}. The VTVH MCD data from the 567 nm peak were fitted to two doublets, and the parameters are given in Table 6. An acceptable fit to the data was only obtainable if g $\approx$ 6 was the ground state. The energy separation of 18.7 cm^{-1} translates into a value of $D = -9.4$ cm^{-1}.

Table 8. Energy Levels and Spins for the 16 Sublevels in the Ground State of CoCo*Ec*MetAP/F

energy [cm^{-1}]	S_{total}, $\lvert M_{s\ total}\rvert$
0	3, 2
3.6	3, 1
13.1	3, 0
26.4	1, 1
35.1	2, 0
112.2	3, 3
137.6	1, 0
137.8	0, 0
139.7	2, 2
148.2	2, 1

The insets to Figure 3b show the magnetization plots for the 495 and 567 nm peaks from CoCo*Ec*MetAP/F. Remarkably, the shapes of the magnetization curves are the same, and both differ from their counterpart peaks in CoCo*Ec*MetAP. This result means that ground states of both Co^{II} ions have changed upon fumagillin complexation, and it is not a result of fumagillin providing a ligand to either metal. The most likely reason is that the Co^{II} ions are now magnetically coupled through the bridging water (or hydroxide), which has been modified by the hydrogen-bond formation to an oxygen on the fumagillin. Accordingly, the VTVH MCD data for the 495 and 567 nm peaks were fitted to the dimer model. The fits are shown in insets to Figure 3b, and the parameters are given in Table 7. The subscript "1" to the ZFS parameters D and E refer to metal ion excited state. Therefore, when fitting the 495 nm data, D_1 refers to the 6-coordinate Co^{II} in the Co_2 site. When fitting the 567 nm data, D_1 refers to the 5-coordinate Co^{II} in the Co_1 site. In these fits it was assumed that the single ion ZFS did not change upon complexation with fumagillin. The fact that the fits were excellent and produce similar results for J confirms the validity of this assumption. In this situation, the fits were very sensitive to D for the 5-coordinate Co^{II} because it is in the same range as J. Just as for the dimer model fit of complex **1** VTVH MCD data, the fits were not sensitive to the value of D for the 6-coordinate Co^{II} as long as it was >40 cm^{-1}. As for the model complex **1**, a reasonable fit was not possible if the sign of D was allowed to be negative for the 6-coordinate Co^{II}. The resulting energy and total M_s for each of the 16 sublevels in the ground-state manifold of CoCo*Ec*MetAP/F are given in Table 8. There are three doublets and two singlets that can be partially populated at

(46) Paulat, F.; Lehnert, N. *Inorg. Chem.* **2008**, *47*, 4963–4976.

Table 9. Summary of Magnetic Coupling in Related Complexes

bridging core	Co···Co [Å]	Co−O−Co [deg]	J [cm^{-1}]	ref
1,$Co_2(\mu\text{-OH})(\mu\text{-1,3-}O_2CCH_3)_2$	3.435[a]	121.3[a]	1.7	this work
MetAP/F,$Co_2(\mu\text{-OH(H)})(\mu\text{-1,3-}O_2CR)_2$	3.1[b]	84[b]	2.9	this work
MetAP,$Co_2(\mu\text{-OH}_2)(\mu\text{-1,3-}O_2CR)_2$	3.2	98	∼0	this work
$Co_2(\mu\text{-OH}_2)(\mu\text{-1,3-}O_2CCH_3)_2$	3.548	113	−0.2	18
$Co_2(\mu\text{-OH}_2)(\mu\text{-1,3-}O_2CCH_3)_2$	3.687	117	−1.6	19
$Co_2(\mu\text{-OH}_2)(\mu\text{-1,3-}O_2CCH_3)_2$	3.597	115	−0.7	20,21
$Co_2(\mu\text{-1,3-}O_2CCH_3)_2(\mu\text{-1,1-}O_2CCH_3)$	3.494	108	18.0	20,47
$Co_2(\mu\text{-AA})(\mu\text{-1,3-}O_2CCH_3)_2$[c]	3.432	111	−3.6	20,48
$Co_2(\mu\text{-OG})(\mu\text{-1,3-}O_2CCH_3)_2$[d]	3.631	127	−1	49
$Co_2(\mu\text{-OPhR})_2$[e]	3.092	97	−6.9	50
$Co_2(\mu\text{-OPhR}')(\mu\text{-1,3-}O_2CCH_3)$[f]	3.505	126	−2.7	51
$Co_2(\mu\text{-OPhR}'')(\mu\text{-1,3-}O_2CCH_3)_2$[g]	3.356	112	−0.2	52
$Co_2(\mu\text{-OPhR}''')(\mu\text{-1,3-}O_2P(OPh)_2)_2$[h]	3.665	126	−1.6	24

[a] Assumed from the crystal structure of **2**. [b] Assumed from the structure of CoCo*Hs*MetAP/F, PDB: 1BOA. [c] AA = acetohydroxamate, $CH_3(C{=}O)N(H){-}O^-$. [d] OG = *N*-oxyglutarimide, $C_5H_6NO_3$. [e] OPhR = 2,6-diformyl-4-methylphenol dioxime. [f] OPhR′ = 2,6-cresolate-*N*,*N*,*N*′,*N*′-tetramethylene carboxylate. [g] OPhR″ = 2,6-bis[bis(2-hydroxyethyl)aminomethyl]-4-methylphenolate (bhmp$^-$). [h] OPhR‴ = 2,6-bis((*N*,*N*′-bis-(2-picolyl)amino)methyl)-4-terbutylphenolato (bpbp$^-$).

the temperatures of the MCD experiment. Doing so requires 25 independent parameters to fit using the singlets/doublets program. With so many parameters, the fits cannot be given too much meaning; however, they were excellent, yielding $g \approx 8$ for the ground state when the data from both the 495 and 567 nm peaks were fitted. The fits and parameters are shown in Figures S9 and S10, Supporting Information.

A change in polarization was again considered for the difference in magnetization behavior of the 495 and 567 nm peaks on formation of the fumagillin complex with CoCo*Ec*MetAP. In this analysis, the 495 and 567 nm VTVH MCD data were fitted using the dimer program with J set to zero and polarization floated. The fits were not as good as those given in Table 7. However, if the polarization was locked to the values obtained after the initial fit with $J = 0$ and then J was floated, the fits improved somewhat. The details are given in Table S1 in the Supporting Information. As opposed to the case for complex **1**, the polarization change hypothesis cannot be entirely ruled out, but a very weak ferromagnetic coupling still is required to achieve an acceptable fit.

Discussion

An understanding of the electronic properties of dinuclear Co^{II} complexes provides insight into the electronic properties and reactivity of dinuclear Co^{II} active sites in enzymes. In this study, the magnitude and sign of magnetic coupling in the $Co^{II}Co^{II}/Co^{II}Co^{III}$ model system informed the analysis of the VTVH MCD data on CoCo*Ec*MetAP and the complex with the fumagillin inhibitor. Unfortunately, we were unable to find reports of other J's for dinuclear Co^{II} μ-hydroxo complexes. There are a few reports of weak antiferromagnetic coupling in μ-aqua complexes with additional acetate bridging ligands from Coucouvanis et al.,[18] Schultz et al.,[19] and Brown et al.[20] with J's ranging from -0.2 to -1.6 cm^{-1} (Table 9). In one of these reports the authors suggest that $|J|$ should increase on going from a μ-aqua bridge to a μ-hydroxo bridge.[19] This possibility is consistent with the J for **1** and might suggest that CoCo*Ec*MetAP has a μ-aqua bridge and, through hydrogen bonding, becomes more "hydroxide like" in CoCo*Ec*MetAP/F.

Ostrovsky et al.,[47,48] Brown et al.,[49] Black et al.,[50] Cai et al.,[51] and Hossain et al.[52] prepared and characterized several dinuclear Co^{II} complexes that have acetate bridging ligands and an additional bridging oxygen atom from another ligand (Table 9). In a very recent report on a dinuclear Co^{II} complex in which the metals are bridged by two diphenyl phosphate bridging groups and a bridging phenolate oxygen atom, VTVH MCD was used to determine J, and the value was confirmed by magnetic susceptibility.[24] The reported coupling constants for these complexes are all in the range of weak antiferromagnetic coupling ($J = -0.2$ to -6.9 cm^{-1}), except for one complex reported to exhibit moderate ferromagnetic coupling ($J = 18.0$ cm^{-1}). Thus, the weak ferromagnetic coupling in **1** and CoCo*Ec*MetAP/F is unusual, but it is certain that these systems are coupled and that coupling is ferromagnetic. The changes in the ground state of Co^{II} when coupling is "switched on" argue the case for magnetic coupling, and the shape of the magnetization curves requires that the coupling be ferromagnetic. Weak ferromagnetic coupling has also been observed in the dicobalt(II)-substituted form of aminopeptidase from *Aeromonas proteolytica* (CoCoAAP).[53] Interestingly, the active site in CoCoAAP consists of a bis(μ-aqua/hydroxo)(μ-carboxylato)dicobalt(II)) core with one 6-coordinate and one 5-coordinate Co^{II}, very similar to that of CoCo*Ec*MetAP and CoCo*Ec*MetAP/F.[54]

Not all reports of magnetic coupling in dinuclear Co^{II} complexes use the same spin Hamiltonian to determine J. Some models have neglected zero-field splitting, which can affect the magnitude of J. In some highly symmetric Co^{II} dimers orbital contributions have been considered after the spin coupling model was shown to be inadequate because of strong orbital contributions through spin−orbit coupling.[47,52,55,56] We do not believe that orbital contributions are important in **1** or CoCo*Ec*MetAP/F because the geometric distortion and ligand heterogeneity both serve to quench the orbital angular momentum in the ground state.[52] This belief is supported by the AOM calculation for Co^{II} in **1**.

The MCD spectra clearly show that both metal sites are occupied in CoCo*Ec*MetAP/F, conflicting with an EXAFS

(47) Ostrovsky, S. M.; Werner, R.; Brown, D. A.; Haase, W. *Chem. Phys. Lett.* **2002**, *353*, 290–294.
(48) Ostrovsky, S. M.; Falk, K.; Pelikan, J.; Brown, D. A.; Tomkowicz, Z.; Haase, W. *Inorg. Chem.* **2006**, *45*, 688–694.
(49) Brown, D. A.; Glass, W. K.; Fitzpatrick, N. J.; Kemp, T. J.; Errington, W.; Clarkson, G. J.; Haase, W.; Karsten, F.; Mahdy, A. H. *Inorg. Chim. Acta* **2004**, *357*, 1411–1436.
(50) Black, D.; Blake, A. J.; Dancey, K. P.; Harrison, A.; McPartlin, M.; Parsons, S.; Tasker, P. A.; Whittaker, G.; Schroder, M. *J. Chem. Soc., Dalton Trans.* **1998**, 3953–3960.
(51) Cai, L.; Xie, W.; Mahmoud, H.; Han, Y.; Wink, D. J.; Li, S.; O'Connor, C. J. *Inorg. Chim. Acta* **1997**, *263*, 231–245.
(52) Hossain, M. J.; Yamasaki, M.; Mikuriya, M.; Kuribayashi, A.; Sakiyama, H. *Inorg. Chem.* **2002**, *41*, 4058–4062.
(53) Bennett, B.; Holz, R. C. *Biochemistry* **1997**, *119*, 1923–1933.
(54) Munih, P.; Moulin, A.; Stamper, C. C.; Bennett, B.; Ringe, D.; Petsko, G. A.; Holz, R. C. *J. Inorg. Biochem.* **2007**, *101*, 1099–1107.
(55) Tsukerblat, B. S.; Palii, A. V.; Mirovitskii, V. Y.; Ostrovsky, S. M.; Turta, K.; Jovmir, T.; Shova, S.; Bartolome, J.; Evangelisti, M.; Filoti, G. *J. Chem. Phys.* **2001**, *115*, 9528–9535.
(56) Fink, K.; Wang, C.; Staemmler, V. *Inorg. Chem.* **1999**, *38*, 3847–3856.

Table 10. Cobalt−Oxygen Angles and Distances in Three CoCoMetAPs

	Co−O−Co [deg]	$Co_1\cdots O$ [Å]	$Co_2\cdots O$ [Å]	Co···Co [Å]	PDB File
CoCo*Hs*MetAP	101	2.00	2.05	3.13	2B3K
CoCo*Ec*MetAP	98	2.14	2.08	3.17	2MAT
CoCo*Hs*MetAP/F	84	2.36	2.13	3.00	1BOA

study that reported evidence that when fumagillin is complexed to CoCo*Ec*MetAP one metal is lost from the active site.[28] On the other hand, these results agree with an EPR study of MnMn*Ec*MetAP/F, which showed both metal sites occupied.[16] All of the spectroscopic studies of fumagillin complexes with MetAP concur that fumagillin does not bind directly to either metal in the active site. A 3.28 Å "bond" was reported between the alcoxide oxygen (released when the ring epoxide of fumagillin is ruptured) and Co_1, but the MCD spectrum shows no evidence for this "bond", and 3.28 Å is too long for any strong bonding interaction.[2]

The intriguing question is the cause of magnetic coupling in the fumagillin complex with CoCo*Ec*MetAP. Magnetic coupling between the Mn^{II} ions is unchanged when MnMn*Ec*MetAP is complexed with fumagillin.[16] It may be that the dicobalt site is more flexible than the dimanganese site or that fumagillin does not hydrogen bond to the bridging aqua/hydroxo ligand. Table 10 lists angles and bond distances from three crystal structures of human and *E. coli* CoCoMetAPs. In the human CoCoMetAP, a large change occurs in both the Co−O−Co angle and the Co−O distances. A similar large change in Co−O−Co angle is probable when fumagillin binds to CoCo*Ec*MetAP, forming the hydrogen bond to the bridging water/hydroxide (Scheme 2). Such angle changes, even small ones, have been shown to have effects on the strength and sign of magnetic exchange coupling.[50]

Acknowledgment. The authors gratefully acknowledge Dr. Nataša Mitić, University of Queensland, Australia, for providing the fittings programs and assistance with their use. The authors acknowledge the National Science Foundation for financial support: grant NSF/RUI CHE0554083. A.D.W. also acknowledges the National Institutes of Health and the National Center for Research Resources for financial support through a Vermont Genetics Network grant.

Supporting Information Available: Equations used in the singlets/doublets and dimer fitting programs, absorption spectrum of the CoCo*Ec*MetAP/F complex, and additional magnetization plots and fits. This material is available free of charge via the Internet at http://pubs.acs.org.

IC8011553